Transient Topographies of Ion Patterned Si(111)

Ari-David Brown and Jonah Erlebacher*
Department of Materials Science and Engineering, Johns Hopkins University, Baltimore, Maryland 21218, USA
Wai-Lun Chan and Eric Chason
Division of Engineering, Brown University, Box D, Providence, Rhode Island 02912, USA
(Received 29 October 2004; revised manuscript received 15 February 2005; published 25 July 2005)

The surface of high fluence ion-sputtered Si(111) was found to exhibit a rich variety of transient one- and two-dimensional topographies that may be exploited as tunable self-organized arrays of nanostructures. Such transient effects are only partially described by analytical models of sputter patterning. However, a discrete atom kinetic Monte Carlo simulation model incorporating curvature-dependent sputtering and surface diffusion reproduces many aspects of the transient morphological evolution, and clarifies the minimal model of sputter patterning.

DOI: 10.1103/PhysRevLett.95.056101 PACS numbers: 68.35.Bs, 68.37.Ps, 81.10.Aj, 81.15.Np

A variety of self-organized nanoscale topographies may appear on surfaces that are simultaneously heated and etched by ion beams. Examples include one-dimensional sputter ripples [1,2], hexagonally packed arrays of quantum dots [3], and dots exhibiting rectangular symmetry [4]. The characteristic length scales of these structures may be readily adjusted by varying easily accessible experimental parameters, e.g., substrate temperature and ion beam current. As these morphologies have been observed on a variety of metal [5], semiconductor [6], and oxide [7] surfaces, the fundamental physics governing these pattern-forming instabilities is believed to be ''material independent.'' For this reason, self-organized morphological evolution during ion etching is envisioned to find important general application in nanostructure fabrication.

In this Letter, we report the observation of a series of time-dependent morphological transitions on elevated temperature oblique-incidence Ar^+ ion-sputtered Si(111) in which three distinct but transient morphologies with well-defined periodicity form (Fig. 1). All experiments used 3 in Si(111) wafers (n type, 0.002–0.005 Ohm cm) controlled to 600–750 °C. The ion beam characteristics are the following: neutralized 500 eV Ar^+ ions oriented 60° from normal; projected beam direction along $[1\bar{1}0]$; beam current density 0.75 mA/cm^2. The three morphologies can be described as a superposition of ripples oriented with the wave vector parallel to (the ''parallel mode'') and perpendicular to (the ''perpendicular mode'') the ion beam. Parallel-mode ripples always appear first and are very well aligned. They possess wavelengths that initially appear between 300–500 nm, and possess very small amplitudes, usually less than 5 nm. During the transition to two-dimensional ripples, less well-aligned perpendicular mode corrugations appear. These corrugations possess larger wavelengths than the parallel-mode ripples, usually greater than 500 nm, and eventually grow to possess larger amplitudes as well, often greater than 20 nm. When the amplitude of each mode is roughly equivalent, the morphology of the surface is that of a rectangular array of mounds, the mound dimensions being determined by the wavelengths of each ripple mode, as shown in Fig. 1(b). Ultimately, the parallel-mode features are obliterated and the surface develops a one-dimensional periodicity orthogonal to the original. Analytical models for the sputter rippling instability have been developed that predict transient pattern evolution, but to our knowledge such evolution has not been seen experimentally, and our results here only share selected features with the predictions of these models.

In situ monitoring of ripple growth was performed using UV light scattering spectroscopy (LiSSp) [1,8]. LiSSp uses a broad band UV light source to illuminate a region of the sample and measures the nonspecular light scattered in a

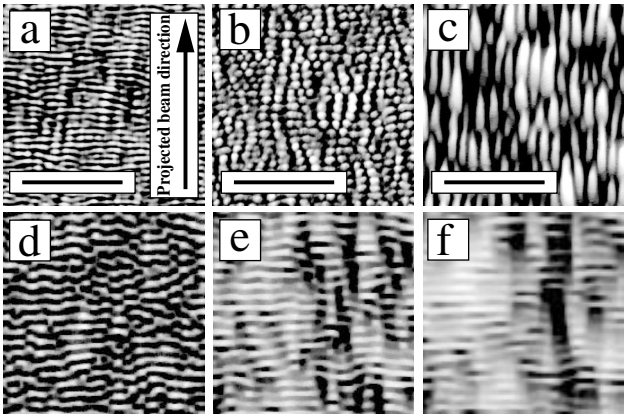

FIG. 1. (a), (b), (c) Atomic force microscope micrographs of sputter rippled Si(111); scale bar = 5 μm; sample temperature = 657 °C. 1D features with mean ripple amplitudes of 3 and 15 nm are observed in (a) (fluence = 8.4×10^{18} ions/cm^2) and (c) (fluence = 4.8×10^{19} ions/cm^2). (b) 2D sputter mounds with amplitude = 7 nm were formed at intermediate ion fluence (2.2×10^{19} ions/cm^2). (d)–(f) Grayscale images of KMC simulations (512×512 regions) illustrating the morphological evolution of a sputtered (100) surface: (d) 12 s, (e) 24 s, and (f) 48 s.

fixed direction. This technique provides a real-time measurement of the morphological power spectrum of the surface topography, because periodic ripples scatter light from a portion of the incident spectrum, acting like a diffraction grating [9]. Figure 2 shows LiSSp-obtained power spectra collected every 1200 s on a sputter-etched sample during the parallel-mode evolution. The peaks are well defined for sputtering time t exceeding 3600 s, indicating that the surface features are highly regular. The decrease in the parallel-mode ripple growth rate at longer sputtering times is evident in the evolution of the spectra. There is also a noticeable decrease in the characteristic corrugation wave vector q_{app} representing an increase in wavelength from ~500 to ~550 nm, during which an increase in amplitude from 2 to 2.5 nm is observed. The empirical form $q_{\mathrm{app}}(t) = Ae^{-\delta t} + C$, where A, C, and δ are fitting parameters, was found to agree well with the data measured in the 600–750 °C temperature range; an example is shown in Fig. 3.

Current analytical models [10–12] for the growth of sputter ripples are enhancements of ideas first discussed by Bradley and Harper (BH) [13]. BH theory takes the idea first expressed by Sigmund [14] that the sputter yield in the valley of a surface perturbation (a negative curvature region) is greater than the sputter yield at its crest (a positive curvature region). This effect leads to roughening during ion beam etching. In addition, the theory incorporates roughening with surface smoothing via surface diffusion [15]. These competing mechanisms drive self-organization of the surface topography; characteristic length scales and periodicity appear, because small features are healed quickly by surface diffusion and large features grow slowly in amplitude. Variations of this model to account for step-edge barriers [11], anisotropic diffusion [5,11], and other nonisotropic surface physics have been developed [10], but we expect the Si(111) surface under our experimental conditions to display none of these features [16–18].

The nonlinear BH model [12] gives the following equation for the surface topography $h(x, y)$, where x points in the direction of the projected ion beam:

$$\frac{\partial h}{\partial t} = -\nu_0 + \phi\frac{\partial h}{\partial x} + \nu_x\left(\frac{\partial^2 h}{\partial x^2}\right) + \nu_y\left(\frac{\partial^2 h}{\partial y^2}\right) + \frac{\lambda_x}{2}\left(\frac{\partial h}{\partial x}\right)^2 + \frac{\lambda_y}{2}\left(\frac{\partial h}{\partial y}\right)^2 - K\nabla^4 h + \eta(x, y, t). \quad (1)$$

Here, ν_0 is the rate of erosion of a flat surface, ϕ is the rate of erosion of an inclined surface, ν_x, ν_y are roughening prefactors determining the anisotropic erosion rate in x, y; λ_x, λ_y control the early stages of nonlinear evolution, and η is noise primarily due to fluctuations in the ion beam current. These ion related coefficients are functions of the ion range a, the longitudinal and lateral straggles, σ, μ, and the ion flux F [12]. The term $K\nabla^4 h$ accounts for surface diffusion driven relaxation according to the classical theory [15]; K is proportional to the surface diffusivity D_S. For Si(111) in the experimental temperature and ion flux range used, we expect all mass transport to occur via surface diffusion. Equation (1) is expected to hold as long as the ion range a is small compared to any surface radius of curvature $1/\kappa$, a condition held for all our results.

In the small slope limit, Eq. (1) may be solved using Fourier methods. One finds that the amplitude h_q of a Fourier mode q of the surface may be expressed in the form $h_q(t) = h_q(0)e^{R_q t}$, where the amplification rate $R_q = -(\nu_x q_x^2 + \nu_y q_y^2) - K(q_x^2 + q_y^2)^2$. If $\nu_x < 0$ or $\nu_y < 0$ roughness increases during sputtering. The fastest growing Fourier mode will result in a sputter ripple with wavelength $\lambda^* = (8K\pi^2/\nu^*)^{1/2}$, where ν^* is the greater of $|\nu_x|$ and $|\nu_y|$. We used SRIM 2003 [19] to estimate values for the ion parameters a, σ, μ and estimate ν_x, ν_y. To calculate a, we projected the longitudinal range into the direction of the

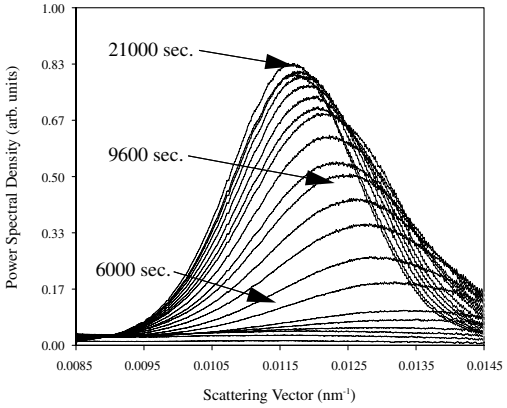

FIG. 2. LiSSp-obtained power spectra of ion-sputtered Si(111) acquired at 1200 s intervals of sputtering time, $T = 725$ °C. It is apparent that ripple coarsening occurs by the shift of peak position toward shorter scattering vector as sputtering time increases.

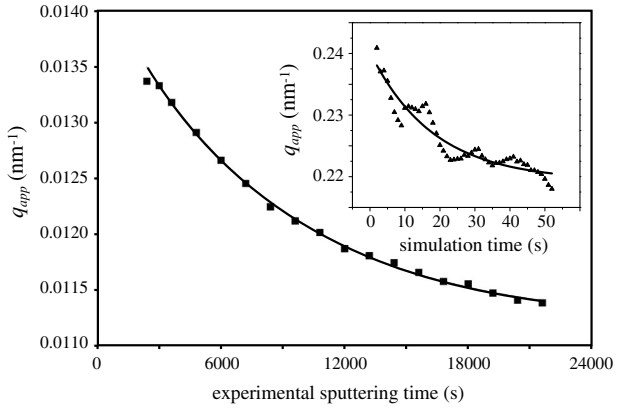

FIG. 3. Evolution of the parallel-mode ripple scattering vector q_{app} with time; the squares represent LiSSp-obtained data and triangles are from our KMC simulation (inset). The lines are fits to the data using offset exponential decays, $q_{\mathrm{app}}(t) = Ae^{-\delta t} + C$.

ion beam; for the straggle parameters σ, μ, we separated the longitudinal straggle into components parallel and perpendicular to the ion beam direction. A reasonable set of values for a, σ, μ was found to be 2.8 nm, 1.6 nm, 0.9 nm, respectively. For this set of values, we find $\nu_x/F = -2.5 \times 10^{-10}$ m and $\nu_y/F = -2.3 \times 10^{-10}$ m. According to the linear theory, these values predict the creation of parallel-mode ripples, in agreement with our observations of ripple evolution during the initial experimental stages.

Analytical predictions of growth evolution in the nonlinear regime are less successful in describing the transient topographies. It has been shown [20] that the sign of $\lambda_x\lambda_y$ is the primary determinant for the morphological evolution of sputtered surfaces after a crossover time t_c. If $\lambda_x\lambda_y < 0$, the surface evolves as described by Eq. (1) and ripples form for $t < t_c$. When $t > t_c$, ripples disappear and the system exists in a randomly rough and transient regime with no long-range order. Interestingly, it is predicted [21] that when the roughness grows sufficiently large, a reentrant, rotated ripple morphology is predicted to appear. These ripples appear at an angle $\theta_c = \tan^{-1}\sqrt{-\lambda_x/\lambda_y}$ relative to the direction of the projected ion beam. If $\lambda_x\lambda_y > 0$, the surface morphology is still described by the linear theory for $t < t_c$ after which the surface undergoes kinetic roughening.

For our experimental conditions, we calculate that $\lambda_x\lambda_y < 0$, which agrees with our experiment insofar as ripples are observed to form. However, the predictions of the nonlinear theory are in contrast to our results in two important ways: (i) We see a rotated ripple topography appear at longer sputtering times. According to the nonlinear theory, the predicted rotation should only be $\sim 25°$ [12], in contrast to our observation of a 90° rotation; (ii) The perpendicular mode rotated topography appears continuously from the background of the parallel-mode ripples with no interval period of random roughness as predicted by the nonlinear theory.

In order to more fully explore the source of this evolution, we developed a kinetic Monte Carlo (KMC) simulation in an attempt to construct a ''minimal model'' for sputter patterning. KMC simulation is an ideal technique for sputter rippling, because the simulated morphologies are nonanalytical solutions for ripple growth that contain all the physical mechanisms in the BH model. This technique can be extended into the nonlinear regime and include cases where step-step interactions are significant and the effect of noise is properly accounted. Other attempts have utilized Monte Carlo methods to model sputter-induced patterning [22–24] but have not always included realistic atomic transport and have not focused on the nonlinear regime.

Our KMC model uses the mechanism for sputter removal of atoms proposed by Sigmund [14] in which the functional form of the deposited energy $E(\bar{r})$ transferred from an implanted ion to a point of implant $\bar{r}$ a distance a into the surface is given by

$$E(\bar{r}) \propto e^{-[(z')^2/2\sigma^2 + (x'^2+y'^2)/2\mu^2]}. \quad (2)$$

The primed reference frame is that used by Makeev, *et al.* [12] to describe the local coordinates of the incident ion relative to the impact point: z' is along the direction of the ion trajectory; x' and y' are orthogonal to it. The parameters a, σ, and μ refer to the range, longitudinal straggle, and radial straggle of the ion as discussed above. The probability that an atom is removed at a particular surface site is proportional to the relative energy deposited at that site as calculated by Eq. (2). Our simulation addresses the variation of the sputter yield with surface roughness (i.e., curved surfaces) by scaling the sputter yield for a flat surface by a factor equal to the ratio of the energy deposited on a rough surface to the energy deposited on a flat surface.

Surface diffusion is described by assigning an Arrhenius-type hopping rate Γ to each surface atom with an activation energy proportional to the local bond coordination [25], i.e., $\Gamma = \nu e^{-(E_d + nE_b)/k_BT}$, where $\nu = 10^{13}$ s^{-1} is the attempt frequency, n is the number of near neighbors on the surface, E_b is a bond energy, and E_d is the activation energy for adatom hopping. We ignore the effects of energy deposited by ions on diffusion as this energy is dissipated quickly relative to the rate of any diffusive event.

The simulation consists of a square lattice of size 2048×512 where the shorter dimension is parallel to the direction of the ion beam, and we present results for a prototypical dataset [26] using ion beam parameters that are scaled values of the a, σ, and μ values we assume for Si in Figs. 1(d)–1(f). These representative simulated topographies may be compared to the experimental ones shown in Figs. 1(a)–1(c). In agreement with experiment, we see the early appearance of a rippled surface topography with the parallel orientation, then saturation of the amplitude of these ripples followed by the appearance of long wavelength features in the perpendicular orientation. Computational limitations preclude the appearance of truly two-dimensional features, but even for our longest runs, the surface has not reached steady state. In addition to the morphological similarity between experiment and simulation, the simulations also yield coarsening of the parallel-mode wavelength with a behavior similar to the experiment (see Fig. 3 inset). Surface mass transport in the simulation is predominantly via surface vacancies; this suggests that a similar mechanism is operative for diffusion on sputtered Si(111).

The apparent independence of the parallel and perpendicular growth modes suggests a growth mode in which the surface initially grows in a traditional BH mode with a dominant parallel mode. Then, at sufficiently high amplitude, nonlinear effects limit further amplitude evolution of the first dominant parallel mode, allowing longer wavelength, more slowly growing parallel modes to become the apparent wavelength, consistent with the observation of

coarsening. This process continues until the parallel-mode growth is so slow that perpendicular mode ripples grow at competitive rates. When the amplitude of parallel and perpendicular mode ripples are roughly equivalent, the perpendicular mode begins to dominate, growing in amplitude until the surface ultimately undergoes kinetic roughening.

Finally, the results presented here for sputtered Si(111) may be contrasted with the results in Ref. [1] for sputtered Si(001), on which was observed only noncoarsening, perpendicular mode ripples under nominally similar experimental conditions. For that study, however, the beam was oriented at a more glancing incidence, below the critical angle separating the two growth modes according to BH theory (which is slightly greater than 60° for silicon), and thus we should only have expected perpendicular mode ripples. This observation highlights the sensitivity of ripple formation on sputtering parameters, for which even ~ 10 degree changes in incidence angle can produce significantly different results. The nature of surface mass transport can also change dramatically; in Si(001), dimers were identified as the likely diffusing species, whereas the simulations here suggest that terrace vacancies are the likely diffusing species.

This work is supported by the United States Department of Energy under Grants No. DE-FG02-01ER45942 (Johns Hopkins University) and No. DE-FG02-0lER45913 (Brown University).

*Corresponding author.
Electronic address: Jonah. Erlebacher@jhu.edu

[1] J. Erlebacher, M. J. Aziz, E. Chason, M. B. Sinclair, and J. A. Floro, Phys. Rev. Lett. **82**, 2330 (1999).
[2] J. Erlebacher, M. J. Aziz, E. Chason, M. B. Sinclair, and J. A. Floro, J. Vac. Sci. Technol. A **18**, 115 (2000).
[3] S. Facsko, T. Dekorsy, C. Koerdt, C. Trappe, H. Kurz, A. Vogt, and H. L. Hartnagle, Science **285**, 1551 (1999).
[4] F. Frost and B. Rauschenbach, Appl. Phys. A **77**, 1 (2003).
[5] S. Rusponi, G. Constantini, C. Boragno, and U. Valbusa, Phys. Rev. Lett. **81**, 4184 (1998).
[6] E. Chason, T. M. Mayer, B. K. Kellerman, D. T. McIlroy, and A. J. Howard, Phys. Rev. Lett. **72**, 3040 (1994).
[7] C. C. Umbach, R. L. Headrick, and K.-C. Chang, Phys. Rev. Lett. **87**, 246104 (2001).
[8] E. Chason, M. B. Sinclair, J. A. Floro, J. A. Hunter, and R. Q. Hwang, Appl. Phys. Lett. **72**, 3276 (1998).
[9] J. M. Elson, Phys. Rev. B **30**, 5460 (1984).
[10] G. Carter and V. Vishnyakov, Phys. Rev. B **54**, 17647 (1996).
[11] S. Rusponi, G. Constantini, C. Boragno, and U. Valbusa, Phys. Rev. Lett. **81**, 2735 (1998).
[12] M. A. Makeev, R. Cuerno, and A.-L. Barabasi, Nucl. Instrum. Methods Phys. Res., Sect. B **197**, 185 (2002).
[13] R. M. Bradley and J. M. E. Harper, J. Vac. Sci. Technol. A **6**, 2390 (1988).
[14] P. Sigmund, J. Mater. Sci. **8**, 1545 (1973).
[15] W. W. Mullins, J. Appl. Phys. **30**, 77 (1959); C. Herring in *The Physics of Powder Metallurgy*, edited by W. E. Kingston (McGraw-Hill, New York, 1959), Chap. 8.
[16] H. C. Jeong and E. D. Williams, Surf. Sci. Rep. **34**, 171 (1999).
[17] S. Kodiyalam, K. E. Khor, and S. Das Sarma, Phys. Rev. B **53**, 9913 (1996).
[18] E. D. Williams, E. Fu, Y.-N. Yang, D. Kandel, and J. D. Weeks, Surf. Sci. **336**, L746 (1995).
[19] J. F. Ziegler and J. P. Biersack, computer code SRIM-2003.20, 2003.
[20] S. Park, B. Kahng, H. Jeong, and A.-L. Barabasi, Phys. Rev. Lett. **83**, 3486 (1999).
[21] M. Rost and J. Krug, Phys. Rev. Lett. **75**, 3894 (1995).
[22] I. Koponen, M. Hautala, and O.-P. Sievanen, Phys. Rev. Lett. **78**, 2612 (1997).
[23] A. K. Hartmann and R. Kree, Phys. Rev. B **65**, 193403 (2002).
[24] M. Stepanova and S. K. Dew, Appl. Phys. Lett. **84**, 1374 (2004).
[25] E. Chason and B. W. Dodson, J. Vac. Sci. Technol. A **9**, 1545 (1991).
[26] Ion beam parameters of $a = 16.37$, $\sigma = 9.35$, $\mu = 5.26$, diffusion energies of $E_d = 0.8$ eV and $E_b = 0.2$ eV, $\theta = 60°$, and a simulation temperature equal to 460 K were used.